Journal of Biomechanics 42 (2009) 1553–1559

Contents lists available at ScienceDirect

Journal of Biomechanics

journal homepage: www.elsevier.com/locate/jbiomech
www.JBiomech.com

Validation of computational fluid dynamics methodology used for human upper airway flow simulations

Goutham Mylavarapu [a], Shanmugam Murugappan [b], Mihai Mihaescu [a], Maninder Kalra [c,*], Sid Khosla [b], Ephraim Gutmark [a,c]

[a] Department of Aerospace Engineering and Engineering Mechanics, University of Cincinnati,United States
[b] Department of Otolaryngology–Head and Neck Surgery, University of Cincinnati,Medical Center, United States
[c] Division of Pulmonary Medicine, Cincinnati Children's Hospital Medical Center, Cincinnati, OH 45229-3039 , United States

ARTICLE INFO

Article history:
Accepted 8 March 2009

Keywords:
Pharyngeal airway
Obstructive sleep apnea
CFD
Validation

ABSTRACT

An anatomically accurate human upper airway model was constructed from multiple magnetic resonance imaging axial scans. This model was used to conduct detailed Computational Fluid Dynamics (CFD) simulations during expiration, to investigate the fluid flow in the airway regions where obstruction could occur. An identical physical model of the same airway was built using stereo lithography. Pressure and velocity measurements were conducted in the physical model. Both simulations and experiments were performed at a peak expiratory flow rate of 200 L/min. Several different numerical approaches within the FLUENT commercial software framework were used in the simulations; unsteady Large Eddy Simulation (LES), steady Reynolds-Averaged Navier-Stokes (RANS) with two-equation turbulence models (i.e. $k-\varepsilon$, standard $k-\omega$, and $k-\omega$ Shear Stress Transport (SST)) and with one-equation Spalart–Allmaras model. The CFD predictions of the average wall static pressures at different locations along the airway wall were favorably compared with the experimental data. Among all the approaches, standard $k-\omega$ turbulence model resulted in the best agreement with the static pressure measurements, with an average error of ~20% over all ports. The highest positive pressures were observed in the retroglossal regions below the epiglottis, while the lowest negative pressures were recorded in the retropalatal region. The latter is a result of the airflow acceleration in the narrow retropalatal region. The largest pressure drop was observed at the tip of the soft palate. This location has the smallest cross section of the airway. The good agreement between the computations and the experimental results suggest that CFD simulations can be used to accurately compute aerodynamic flow characteristics of the upper airway.

1. Introduction

Obstructive Sleep Apnea (OSA) is a common disorder characterized by recurrent episodes of pharyngeal airway collapse and obstruction during sleep, resulting in repeated episodes of airflow cessation, oxygen desaturation, and sleep disruption (Guilleminault et al., 1976). OSA is reported to affect approximately 4% of the United States population (Young et al., 1993). When untreated, this disorder is associated with morbidity affecting multiple organ systems (Ayappa and Rapoport, 2003).

Both airway anatomic characteristics and abnormal neuromuscular control of the airway have been implicated in the pathogenesis of OSA (Ryan and Bradley, 2005). Among anatomical factors, airway narrowing has been reported in both pediatric and adult subjects with OSA (Arens et al., 2003). The structural changes of narrowed upper airway could additionally predispose the airway to collapse. A better understanding of the unsteady flow field inside the airway, will allow us to characterize the airflow and pressure forces associated with airway narrowing in an OSA patient.

Recently, Computational Fluid Dynamics (CFD) has been utilized to characterize the fluid flow in human airway models. These airway models were reconstructed from magnetic resonance (MR) or computed tomography (CT) imaging data of patients with OSA (Allen et al., 2004; Sung et al., 2006; Xu et al., 2006; Jeong et al., 2007; Gemci et al., 2008; Mihaescu et al., 2008a). CFD has gained significant interest in both the engineering and medical community because of its non-invasive nature. It enables to predict the fluid flow characteristics when one or multiple input flow variables (such as mean inspiratory/expiratory flow rate, breathing rate, input flow turbulence, and lung pressure) are varied. Furthermore, it allows investigation of

* Corresponding author. Tel.: +1 513 636 6771; fax: +1 513 636 4615.
E-mail address: maninderkalra@gmail.com (M. Kalra).

0021-9290/$ - see front matter © 2009 Elsevier Ltd. All rights reserved.
doi:10.1016/j.jbiomech.2009.03.035

different flow variables and fluid forces to a level of fine detail. This might be a limitation for in-vivo, in-vitro or mechanical airway experimental models. Most of the work listed above on upper airway modeling used laminar or steady Reynolds-Averaged Navier-Stokes (RANS) models to compute the airway flow characteristics. Although the computational costs of using these models are low, they fail to accurately predict anisotropic flows (Wilcox, 1993). The upper airway geometry has an irregular shape with bends and area variations, which shows features such as laminar to turbulent transition, adverse pressure gradients, secondary flow regions, and recirculation zones. These numerical algorithms lack the ability to accurately predict such features which are important in understanding the unsteady aerodynamic forces that act on the airway wall. Direct Numerical Simulation (DNS), on the other hand, is a high fidelity approach that solves the complete range of flow scales down to the dissipative level, but it is computationally expensive and time consuming for moderate to high Reynolds number flows. A compromise between the RANS and DNS formulations is Large Eddy Simulation (LES) methodology, which resolves the most energetic flow scales (entering into the inertial sub-range) and models of only the smallest dissipative scales (Pope, 2000). Steady RANS (with both $k-\varepsilon$ and $k-\omega$ models) and unsteady LES predictions of the upper airway flow characteristics were compared by Mihaescu et al. (2008b). It was shown that the computationally expensive LES should be the preferred tool to capture relevant airway-related flow features, which steady RANS cannot reproduce in the flow separation regions downstream of a constricted area. However, their data shows that the $k-\omega$ results were closer to LES results (Mihaescu et al., 2008b).

To gain confidence in the CFD computations, the methodology needs to be validated with either experimental data or benchmark clinical data. Due to the absence of direct accurate invasive clinical flow measurements in upper airways, the validation of the CFD methodology in the present study is performed by comparing with experimental flow data measured in an identical physical model of the airway at same flow conditions.

2. Methods

2.1. MRI data acquisition

Magnetic resonance images were obtained on a 1.5 T MR scanner (Sigma Excite, GE Medical Systems, WI, USA) at the Department of Radiology, Cincinnati Children's Hospital. MR images were acquired when the patient was in supine position with his neck perpendicular to the Frankfort plane, and secured in this position using a soft padding material between neck and coil. The patient was awake during the entire study and was instructed not to move the neck position. Traverse MRI sequences (Axial T1) were obtained spanning the entire pharyngeal length from the roof of the nasal cavity to the lower mandibular plane. Other technical parameters were Field of View (FOV) of 220 mm × 220 mm; 256 × 256 matrix with a pixel resolution of 0.86 mm × 0.86 mm and a slice thickness of 5 mm, and zero spacing between the sequences and fTR/TE = 400/14.

2.2. Construction of airway model

A three-dimensional (3D) anatomically accurate patient-specific model was reconstructed from the axial T1 series using medical imaging software, MIMICS® (Materialise, Belgium). The entire series was loaded into MIMICS and the airway was identified in each of the axial images based on a pre-defined thresholding (in Hounsfeld units-HU) relative to the surrounding tissue. The HU scale range from −1024 to 3056 for MR axial scans used in this study. Masks with pre-defined HU (lower threshold 192 and upper threshold 465) containing airway voxels are grouped in each of the axial images. 3D raw models were reconstructed from these masks by surface triangulation and then exported into REMESHER, another MIMICS module to: (a) demarcate individual faces of inlet, outlet, and wall from the 3D surface model, and (b) improve the surface mesh quality by smoothing and re-meshing, to control the maximum cell edge length and the grid density. This remeshed surface was then scaled to twice the actual size (2:1) and used for generating the numerical and the experimental 3D volume models. The larger scale model provided better access and spatial accuracy for mounting sensors and acquiring flow and pressure measurements. The entire process is outlined in Fig. 1.

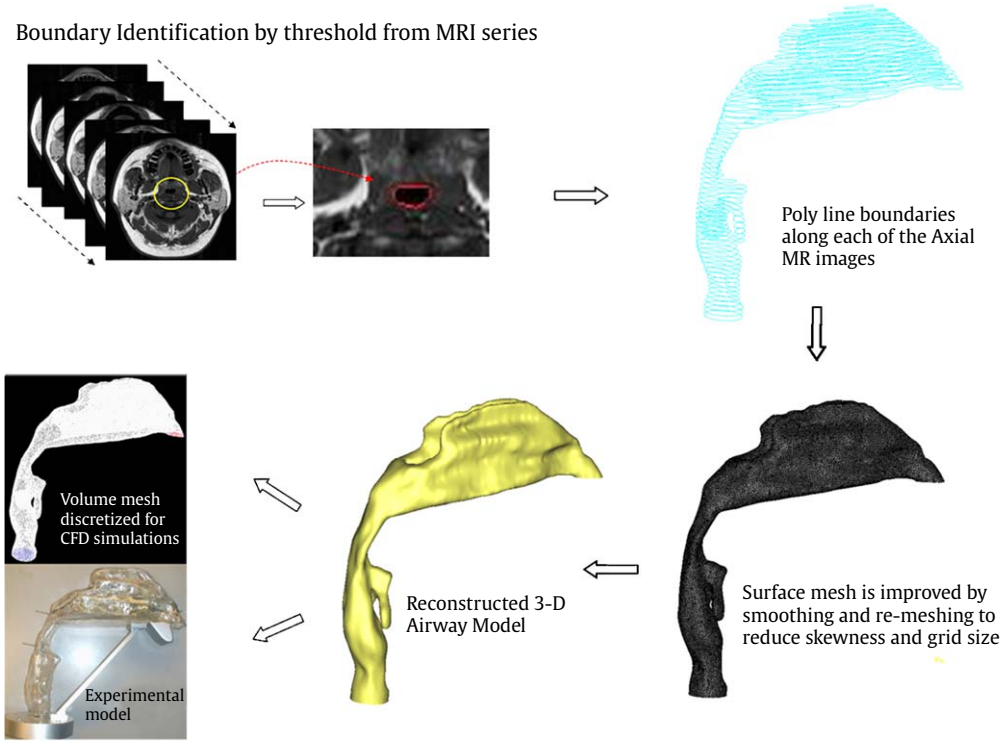

Fig. 1. Process outline—3D airway reconstruction from MRI axial scans.

2.3. Experiments

The 2:1 scaled mechanical airway model was fabricated by Stereo Lithography (STL) process using SLA resin (Somos Watershed 11,110) material for the airway wall yielding nearly uniform thickness. The airway inlet from the tracheal side was connected to the air supply through a settling chamber, a 6° diffuser, and a nozzle. The smooth nozzle provided an area reduction of 12 to 1, to minimize turbulence and laminarize the flow. A 19 mm section provided smooth transition from the circular nozzle exit to the airway inlet. A lip-shaped extension was mounted at the nostril exit to direct the flow exiting the nostrils (Fig. 2). Sixteen pressure taps of 1/16″ diameter were distributed along the walls of the CT-generated 3D airway model (Fig. 3). Nine pressure ports (P1–P9) were located along the posterior side of the pharyngeal airway wall. Four ports (P7, P7L, P7R, and P7A) were placed circumferentially every 90° at the minimum cross-sectional area of the airway. In Figure. 3, A, R, and L refer to the anterior, right, and left positions. Pressure ports P10 to P13 were placed along the lateral walls of the nasal cavity. Ports P1–P5 were positioned at the retroglossal region and ports P6–P8 were located at the retropalatal region. Experiments were performed with an expiratory flow rate of 200 L/min. Flow rates lower than 200 L/min were not tested, since the measured static wall pressure values were below the pressure sensors sensitivity range. The air supply line includes a pressure regulator, one-way flow valve, thermocouple, and a Coriolis flow meter (to measure air flow rate). A Sensotec Gage Pressure Transducer (FPG1WA, Honeywell, Columbus, USA) with an accuracy of ±0.1% and a range of 0–5 in. of water and 0–5 VDC output was used to measure the wall static pressures at each of the 16 ports along the airway model wall. A single probe hotwire (AA Laboratories, Israel) was used to measure velocities at the nozzle exit before entering airway model in this study.

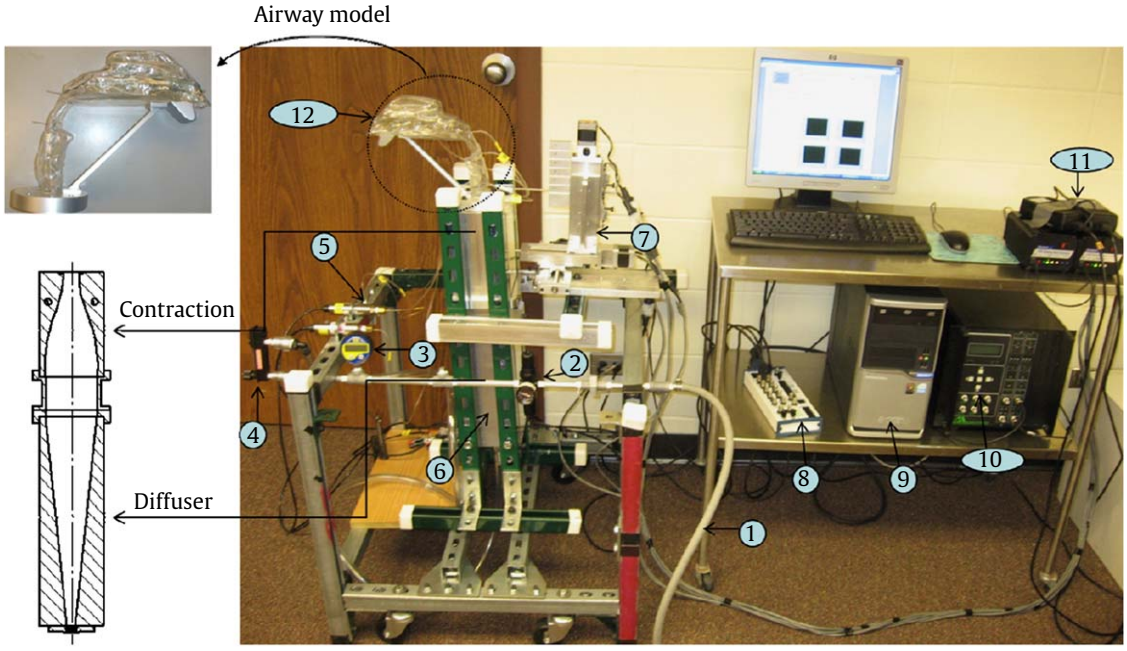

Fig. 2. Experimental setup for pressure and velocity measurements in the airway model. (1) Air Supply; (2) Pressure Regulator; (3) Digital Pressure meter; (4) Flow meter with control valve; (5) Pressure transducers; (6) Diffuser & Contraction Assembly; (7) Traverse; (8) NI DAQ board; (9) Computer; (10) Anemometry System; (11) Traverse motor controller; (12) Airway model.

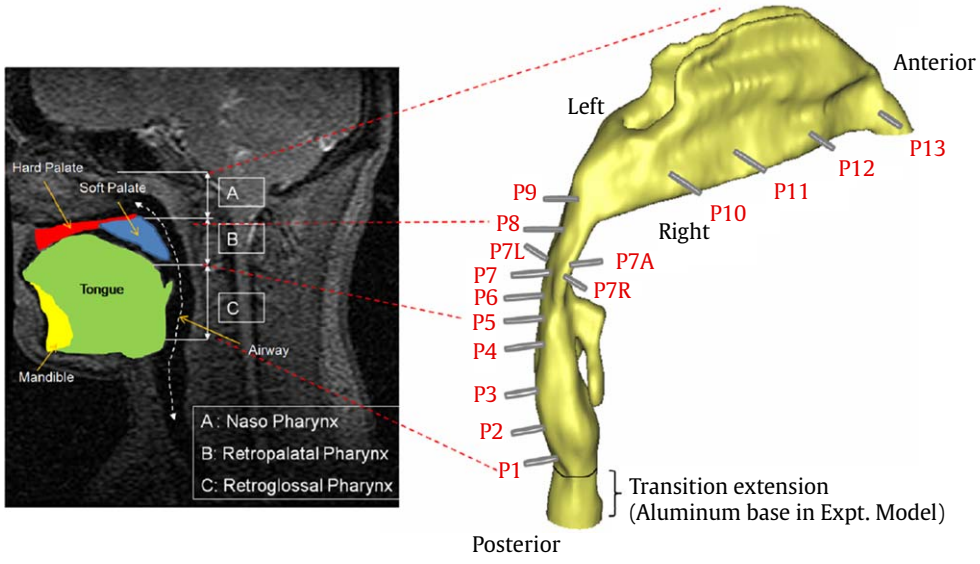

Fig. 3. Experimental airway model with pressure port locations shown. (Sagittal image shown for reference—model not to scale.)

2.4. CFD modeling

2.4.1. Pre-processor

In order to obtain an accurate representation of the mechanical airway model, high spatial resolution axial CT scans (pixel resolution 0.39 mm × 0.39 mm) of the mechanical airway model were obtained. This allowed refining the three-dimensional shape of the airway to precisely represent the physical model for the CFD analysis. MIMICS software was used to generate the numerical airway model and mesh the walls of the airway. A CFD pre-processor, TGRID (Ansys, Lebanon, USA) was then used to create an unstructured tri/tetrahedral hybrid volume mesh with $\sim 55 \times 10^4$ cells inside the airway lumen from $\sim 11 \times 10^4$ triangular faces of the surface mesh on the airway wall.

2.4.2. Flow solver & boundary conditions

Commercial CFD package, Fluent 6.3 (Ansys, Lebanon, USA) was used to solve the airway flow governing equations. Flow simulations were performed during expiration for a peak flow rate of 200 L/min. Ambient static pressure conditions were set at the outlet of the computational domain (nostrils plane). No-slip-wall boundary conditions were imposed on the airway walls. An inlet turbulence intensity of 10% and an estimated turbulent length scale (τ) of 1 mm were selected for the simulations. Five different CFD numerical models within the FLUENT framework were investigated. These included unsteady LES, steady RANS with two-equation turbulence models (i.e. $k-\varepsilon$, standard $k-\omega$, $k-\omega$ Shear Stress Transport (SST) and with one-equation Spalart–Allmaras model. The very low Mach number airflow (Mach $\ll 0.3$) justified the assumption of flow incompressibility. The discretization of the flow governing equations on the computational domain was performed using second-order finite-volume schemes. Second-order implicit discretization was employed for time integration. In all these formulations, the coupling between the pressure and the velocity field was implemented through a SIMPLE algorithm (Van Doormaal and Raithby, 1984). In the LES calculations, the WALE sub-grid scale (SGS) model is employed. The LES results were statistically averaged for a period of roughly 60 flow-through times (8000 time steps), achieving a converged solution at each time step. The time step used in this study is 1.5e−4 s.

3. Results

The patient in this study is a male adolescent (17 years old with BMI 26 kg/m^2). Reynolds number for the flow rate of 200 L/min in this 2:1 scaled airway model is ~8500 at inlet and ~18,400 at the site of minimum cross-sectional area. Fig. 4 shows the measured inlet mean velocity profile at the exit of the nozzle before entering the airway. The "top-hat" profile showed that a uniform airflow was fed into the experimental model and thus justified the inlet boundary condition selected in the numerical simulations. A low turbulence air flow with turbulence intensity, less than 3% was achieved with the design of the air-conditioning assembly upstream of the airway.

Figs. 5 and 6 show a bar-graph of time-averaged wall static pressure values measured at the pressure ports and the corresponding predictions by all the five CFD models, at an expiratory peak flow rate of 200 L/min. The error bars associated with the experimental measurements are also marked in the figures. The static pressure at the posterior side of the airway wall decreased in the flow direction from the epiglottis level to pressure port P6. The pressure changed sign at the location P7 that corresponds to the maximum airway narrowing. The pressure recovers downstream of the minimum cross-sectional area due to the geometrical expansion of the respiratory tract and remained around 38 Pa on the lateral walls of the nasal cavity. All the numerical models used, show a similar trend to that obtained by the experiments, except for the monitoring position P6 where all models predicted positive time-averaged pressures, while the experimental value was negative. This port was at the location where the retroglossal airway splits into vallecula, thus causing separated unsteady flow that is difficult to accurately capture by these models. Unsteady LES was able to pick instantaneous negative and positive pressures at P6, although the time-averaged static pressures remained positive as shown in Fig. 7. Steady RANS

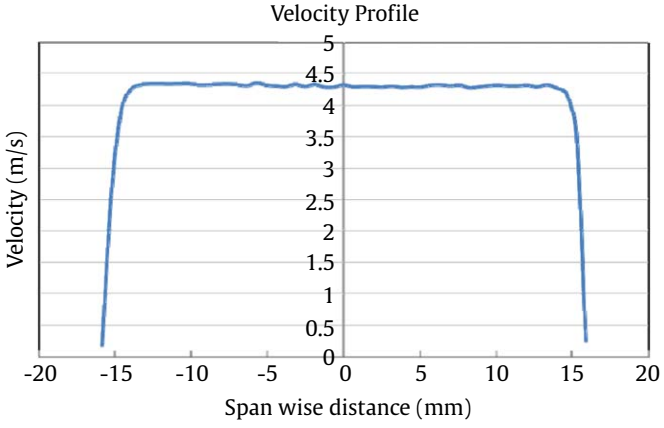

Fig. 4. Measured velocity profile at nozzle exit of the air-conditioning chamber for an expiratory peak flow rate of 200 L/min.

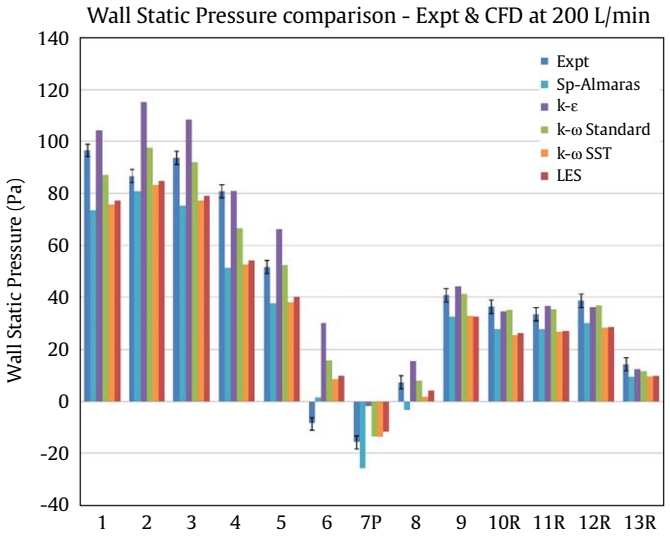

Fig. 5. Comparison of wall static pressure (at the pressure ports shown in chart) between experiments and three different CFD models for an expiratory peak flow rate of 200 L/min.

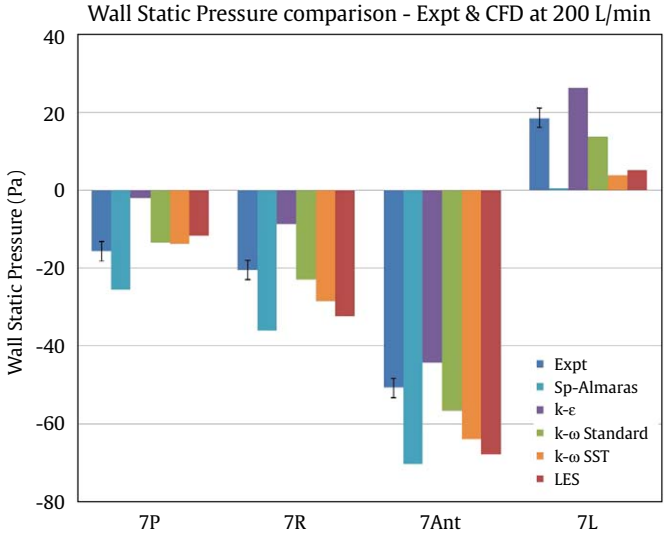

Fig. 6. Comparison of wall static pressure between experiments and three different CFD models at four different ports around the site of minimum cross section for an expiratory peak flow rate of 200 L/min.

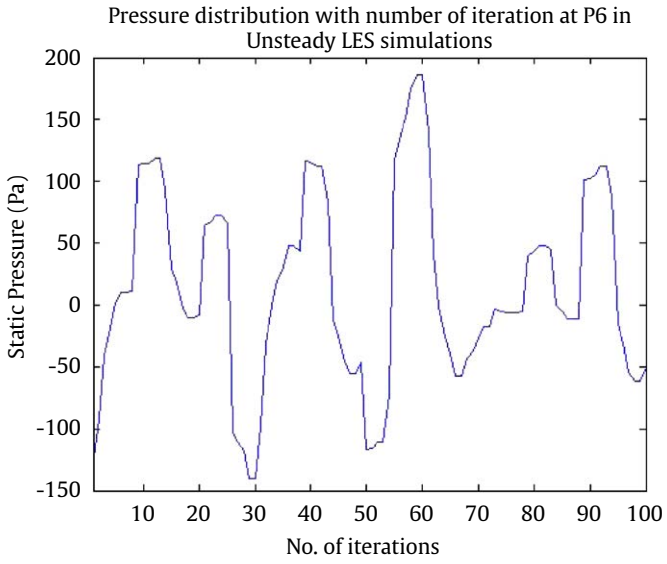

Fig. 7. Instantaneous static pressure distribution with number of iterations in unsteady LES simulations at an expiratory peak flow rate of 200 L/min at pressure port P6.

with standard $k-\omega$ turbulence model yielded better agreement with the experimental data as compared to the other CFD models, when the percentage difference in wall static pressures between predicted and measured values, at each of the pressure ports are compared. The $k-\varepsilon$ model tends to over-predict the pressure values relative to the experimental values at most of the monitoring pressure ports, while the Spalart–Allmaras one-equation turbulence model under-predicts the values compared to the experimental values. Unsteady LES and steady RANS with $k-\omega$ SST model, also under-predict the experimental measurements within roughly 30% average error over all ports. This may be explained by the fact that the grid resolution has to be increased when using LES or $k-\omega$ SST model. The SST model is recommended for high-accuracy boundary layer simulations and requires a very good resolution of the grid nearby the boundary, while the LES requires that the grid size should be of the same order of magnitude or lower than the estimated Taylor micro-scale. The largest discrepancies between the experimental data and the CFD results were observed near the site of minimum cross-sectional area. Fig. 6 presents the measured wall static pressures and the corresponding CFD data at this site. It should be pointed out that there is a marked variation of the wall static pressure around the circumference of the airway. The highest

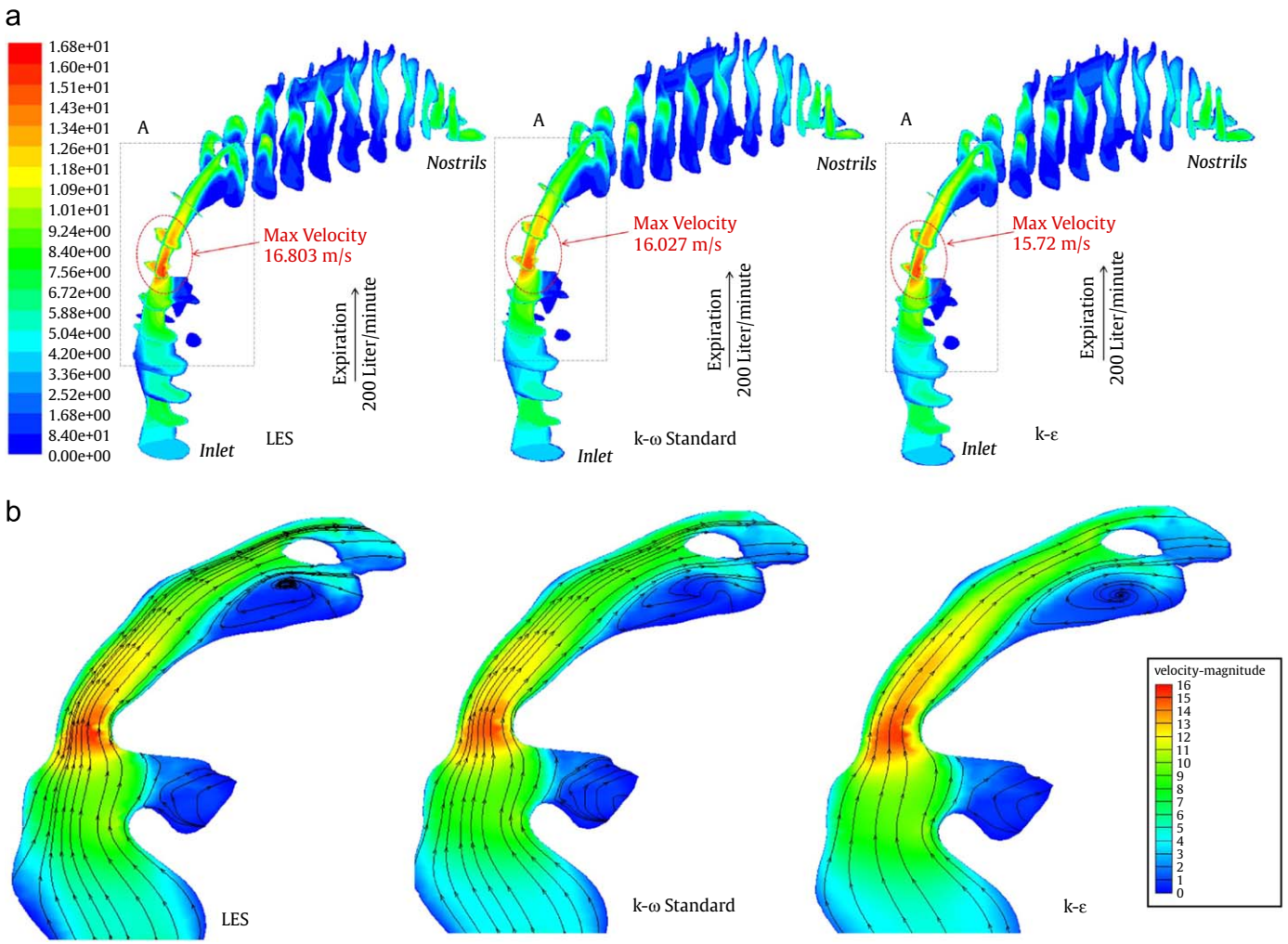

Fig. 8. (a) Contours of time-averaged velocity magnitude at few cross sections along the airflow and in the mid-longitudinal plane for unsteady LES, steady RANS standard $k-\omega$, and $k-\varepsilon$ simulations at an expiratory peak flow rate of 200 L/min. (b) Streamline distribution plot in zone A (marked in Fig. 8a) of the airway in the mid-longitudinal plane for unsteady LES, steady RANS standard $k-\omega$, and $k-\varepsilon$ simulations at an expiratory peak flow rate of 200 L/min.

negative pressure was measured at the anterior section of the airway. The closest numerical results to the experimental measurements within 20% were obtained by the standard $k-\omega$ turbulence model.

Fig. 8a shows the averaged velocity magnitude contour plot at few cross sections along the airflow and in the mid-longitudinal plane with unsteady LES and steady RANS with standard $k-\omega$ and $k-\varepsilon$ models. Although major differences were not observed in the flow distribution along this geometry, unsteady LES picked stronger recirculation regions than the standard $k-\omega$ model as observed in Fig. 8b. The streamlines are plotted in the mid-longitudinal plane of the airway in Fig. 8b.

4. Discussion

The current CFD simulations and experimental measurements in the present airway model indicate the three-dimensional nature of the airflow and the corresponding pressure distribution on the airway wall. This enables us to quantify the interaction between airway anatomy and airway dynamics. Earlier work on the airway which utilized 1D and 2D analysis cannot predict such behavior (Aittokallio et al., 2001; Malhotra et al., 2002). The current study on an anatomically accurate airway emphasizes the complexity of the flow relations in the upper airway. This is a critical first step that would help us better understand the pathogenesis of airway disorders such as OSA.

The non-invasive CFD modeling allows investigation of a wide variety of flow situations under which pressure and stress parameters in the airway can be monitored. The current study uses steady RANS and unsteady LES approaches to model the airflow, the predictions, and trends of wall static pressure that were found to be reasonable as compared to the experimental results. Among the five different turbulence models used in the study, the standard $k-\omega$ model predictions were the closest to experimental results. This is attributed partly to the better treatment of adverse pressure gradient and viscous near-wall region with $k-\omega$ turbulence model as compared to $k-\varepsilon$ and the Spalart–Allmaras one-equation model (Wilcox, 1993). From the past work by Mihaescu et al. (2008b), at least the same or a better level of agreement with the experimental measurements is expected, when LES approach is used. The present LES calculation shows decent agreement with the experimental measurements at selected monitoring points, even if the LES was performed on a coarse grid resolution. This in fact explains the differences between the two data sets. Further experimental studies with velocity measurements in the airway model are required to validate the secondary flow features picked up by the LES simulations.

The etiology of OSA is multifactorial, consisting of a complex interplay between anatomic and neuromuscular factors. Several studies in adults have shown that subjects with OSA have a narrow upper airway as compared to age-matched controls. This anatomic difference has been reported both during sleep and while awake. Extending these findings to the pediatric population, it was shown in the past using static MR images, that the upper airway in children with OSA is narrower during sleep than that of controls (Arens et al., 2001). The role of non-structural factors in the etiology of OSA is supported by the changes in sleep–wake manifestations of this disorder, with patients symptomatic only during sleep. The study of airway dynamics has been hampered by the risk of radiation exposure (fluoroscopy) or invasive techniques. Availability of non-invasive tools, such as computational modeling of airway models has furthered our understanding of the interaction between airway anatomic characteristics and airway predisposition to collapse in the pathogenesis of OSA. Additionally, such tools are being utilized to predict response to OSA treatment. A recent study demonstrated the use of 3D computational simulations of rigid airway models before and after surgical treatment for OSA to differentiate between treatment responders and non-responders (De Backer et al., 2007). Our results are highly significant for such investigations as they not only validate the computational simulations but also can be used to guide the selection of the numerical model.

Though there are numerous turbulence models available within the FLUENT framework, current study clearly indicates that there is a need to validate the model with experimental data for such complex flow simulations. In this study, Spalart–Allmaras model performed poorly when compared to the other turbulence models in predicting flow pressures, whereas RANS with standard $k-\omega$ model performed favorably in predicting experimental measurements. This does not indicate that the one-equation numerical model is flawed. It just indicates that the inadequacy in capturing the fluid flow behavior in a complex-shaped airway requires fine tuning of the model coefficients for a better performance. Though there were variations between the different models, one of the clear advantages of using CFD is that it is able to better predict fluid flow characteristics and trends in the complex aerodynamic flow behavior inside the airway. This cannot be achieved from simplified one-dimensional Bernoulli equation and requires solution of the Navier-Stokes equation using the CFD methodology described in this study.

5. Conclusions

In past years, several studies have shown the use of CFD in better understanding biological flows, especially in human airways (Keyhani et al., 1995; Jeong et al., 2007; Gemci et al., 2008). Few of such studies have shown validation of their CFD methodology (Allen et al., 2004; Croce et al., 2006; van Ertbruggen et al., 2008). However, due to limitation that arises due to inaccessibility, inaccuracy, and invasiveness of clinical measurements, it is challenging to validate computational results. In the current study, flow pressure measurements in an experimental model were compared with numerical results predicted by different turbulence models within the FLUENT framework. It was found that standard $k-\omega$ turbulence model is a better predictor of the experimental measurements of wall static pressures in this patient-specific geometry, followed by LES and $k-\omega$ SST models. The current study provides confidence that CFD can be used to accurately model complex airway flow behavior. It also allowed us to identify a non-expensive numerical formulation that can predict accurately the flow characteristics associated with the upper airway, this being the first step in understanding the mechanisms that govern airway obstruction in OSA.

Conflict of interest

None of the authors have any financial and personal relationships with other people or organizations that could inappropriately influence (bias) their work.

Acknowledgements

This study was supported by the URC interdisciplinary grant "Quantifying the upper airway flow characteristics in Obstructive Sleep Apnea (OSA): Diagnostic and Therapeutic Applications". The authors would also like to acknowledge the technical support provided for image processing by MIMICS® (Materialise, Belgium).

References

Aittokallio, T., Gyllenberg, M., Polo, O., 2001. A model of a snorer's upper airway. Mathematical Biosciences 170 (1), 79–90.

Allen, G.M., Shortall, B.P., Gemci, T., Corcoran, T.E., Chigier, N.A., 2004. Computational simulations of airflow in an in-vitro model of the pediatric upper airways. Journal of Biomechanical Engineering 126 (5), 604–613.

Arens, R., McDonough, J.M., Corbin, A.M., Rubin, N.K., Carroll, M.E., Pack, A.I., Liu, J., Udupa, J.K., 2003. Upper airway size analysis by magnetic resonance imaging of children with obstructive sleep apnea syndrome. American Journal of Respiratory and Critical Care Medicine 167 (1), 65–70.

Arens, R., McDonough, J.M., Costarino, A.T., Mahboubi, S., Tayag-Kier, C.E., Maislin, G., Schwab, R.J., Pack, A.I., 2001. Magnetic resonance imaging of the upper airway structure of children with obstructive sleep apnea syndrome. American Journal of Respiratory and Critical Care Medicine 164 (4), 698–703.

Ayappa, I., Rapoport, D.M., 2003. The upper airway in sleep: physiology of the pharynx. Sleep Medicine Reviews 7 (1), 9–33.

Croce, C., Fodil, R., Durand, M., Sbirlea-Apiou, G., Caillibotte, G., Papon, J.-F., Blondeau, J.-R., Coste, A., Isabey, D., Louis, B., 2006. In-vitro experiments and numerical simulations of airflow in realistic Nasal airway geometry. Annals of Biomedical Engineering 34 (6), 997–1007.

De Backer, J.W., Vanderveken, O.M., Vos, W.G., Devolder, A., Verhulst, S.L., Verbraecken, J.A., Parizel, P.M., Braem, M.J., Van de Heyning, P.H., De Backer, W.A., 2007. Functional imaging using computational fluid dynamics to predict treatment success of mandibular advancement devices in sleep-disordered breathing. Journal of Biomechanics 40 (16), 3708–3714.

Gemci, T., Ponyavin, V., Chen, Y., Chen, H., Collins, R., 2008. Computational model of airflow in upper 17 generations of human respiratory tract. Journal of Biomechanics 41 (9), 2047–2054.

Guilleminault, C., Tilkian, A., Dement, W.C., 1976. The sleep apnea syndromes. Annual Review of Medicine 27 (1), 465–484.

Jeong, S.-J., Kim, W.-S., Sung, S.-J., 2007. Numerical investigation on the flow characteristics and aerodynamic force of the upper airway of patient with obstructive sleep apnea using computational fluid dynamics. Medical Engineering & Physics 29 (6), 637–651.

Keyhani, K., Scherer, P.W., Mozell, M.M., 1995. Numerical simulation of airflow in the human nasal cavity. Journal of Biomechanical Engineering 117 (4), 429–441.

Malhotra, A., Huang, Y., Fogel, R.B., Pillar, G., Edwards, J.K., Kikinis, R., Loring, S.H., White, D.P., 2002. The male predisposition to pharyngeal collapse: importance of airway length. American Journal of Respiratory and Critical Care Medicine 166 (10), 1388–1395.

Mihaescu, M., Murugappan, S., Gutmark, E., Donnelly, L.F., Khosla, S., Kalra, M., 2008a. Computational fluid dynamics analysis of upper airway reconstructed from magnetic resonance imaging data. Annals of Otology, Rhinology and Laryngology 117 (4), 303–309.

Mihaescu, M., Murugappan, S., Kalra, M., Khosla, S., Gutmark, E., 2008b. Large eddy simulation and Reynolds-averaged Navier-stokes modeling of flow in a realistic pharyngeal airway model: an investigation of obstructive sleep apnea. Journal of Biomechanics 41 (10), 2279–2288.

Pope, S.B., 2000. Turbulent Flows. Cambridge University Press, Cambridge.

Ryan, C.M., Bradley, T.D., 2005. Pathogenesis of obstructive sleep apnea. Journal of Applied Physiology 99 (6), 2440–2450.

Sung, S.J., Jeong, S.J., Yu, Y.S., Hwang, C.J., Pae, E.K., 2006. Customized three-dimensional computational fluid dynamics simulation of the upper airway of obstructive sleep apnea. Angle Orthodontics. 76 (5), 791–799.

Van Doormaal, J.P., Raithby, G.D., 1984. Enhancements of the SIMPLE method for predicting incompressible fluid flows. Numerical Heat Transfer, Part A: Applications 7 (2), 147–163.

van Ertbruggen, C., Corieri, P., Theunissen, R., Riethmuller, M.L., Darquenne, C., 2008. Validation of CFD predictions of flow in a 3D-alveolated bend with experimental data. Journal of Biomechanics 41 (2), 399–405.

Wilcox, D.C., 1993. Turbulence Modeling for CFD. DCW Industries, Inc., La CÃ£nada, CA.

Xu, C., Sin, S., McDonough, J.M., Udupa, J.K., Guez, A., Arens, R., Wootton, D.M., 2006. Computational fluid dynamics modeling of the upper airway of children with obstructive sleep apnea syndrome in steady flow. Journal of Biomechanics 39 (11), 2043–2054.

Young, T., Palta, M., Dempsey, J., Skatrud, J., Weber, S., Badr, S., 1993. The occurrence of sleep-disordered breathing among middle-aged adults. The New England Journal of Medicine 328 (17), 1230–1235.